

The Catalogue of Stellar Parameters from the Detached Double-Lined Eclipsing Binaries in the Milky Way

Z. Eker^{A,*}, S. Bilir^B, F. Soyduğan^{C,D}, E. Yaz Gökçe^B, E. Soyduğan^{C,D}, M. Tüysüz^{C,D},
T. Şenyüz^{C,D}, O. Demircan^{D,E}

^A Akdeniz University, Faculty of Sciences, Department of Space Sciences and Technologies, 07058, Antalya, Turkey

^B Istanbul University, Faculty of Sciences, Department of Astronomy and Space Sciences, 34119, University-Istanbul, Turkey

^C Çanakkale Onsekiz Mart University, Faculty of Sciences and Arts, Department of Physics, 17100 Çanakkale, Turkey

^D Çanakkale Onsekiz Mart University, Astrophysics Research Center and Ulupınar Observatory, 17100 Çanakkale, Turkey

^E Çanakkale Onsekiz Mart University, Faculty of Sciences and Arts, Department of Space Science and Technologies, 17020 Çanakkale, Turkey

* Email: eker@akdeniz.edu.tr

Abstract: The most accurate stellar astrophysical parameters were collected from the solutions of the light and the radial velocity curves of 257 detached double-lined eclipsing binaries in the Milky Way. The catalogue contains masses, radii, surface gravities, effective temperatures, luminosities, projected rotational velocities of the component stars and the orbital parameters. The number of stars with accurate parameters increased 67 per cent in comparison to the most recent similar collection by Torres et al. (2010). Distributions of some basic parameters were investigated. The ranges of effective temperatures, masses and radii are $2750 < T_{eff}(K) < 43000$, $0.18 < M/M_{\odot} < 33$ and $0.2 < R/R_{\odot} < 21.2$, respectively. Being mostly located in one kpc in the Solar neighborhood, the present sample covers distances up to 4.6 kpc within the two local Galactic arms Carina-Sagittarius and Orion Spur. The number of stars with both mass and radius measurements better than 1 per cent uncertainty is 93, better than 3 per cent uncertainty is 311, and better than 5 per cent uncertainty is 388. It is estimated from the Roche lobe filling factors that 455 stars (88.5 per cent of the sample) are spherical within 1 per cent of uncertainty.

Keywords: Stars: fundamental parameters – Stars: binaries: eclipsing – Stars: binaries: spectroscopic – Astronomical Data based: catalogues

Introduction

Nearly sixty percent or more of the Solar neighborhood stars are binaries or multiple systems (Duquenois & Mayor 1993). Binaries are important for astrophysicists not only because they over populate single stars, but also because they provide basic stellar parameters as independent observed quantities used in testing astrophysical theories. Stellar masses can be determined directly via application of Kepler's law for the visual binaries if apparent orbital parameters were calibrated to be real. A calibration is possible for a visual pair if its distance (parallax) is known. Reliable stellar masses could also be obtained from the radial velocity curves without distance, but only if orbital inclinations were known. The resolved double stars (visual binaries confirmed to be spectroscopic binaries), therefore, are a special case to provide reliable stellar masses, since the orbital inclinations are from the apparent orbit and the absolute orbital sizes are from the radial velocity curves.

Gainfully, the light curves of eclipsing binaries could provide orbital inclinations and the radii relative to the semi-major axis of the orbit. But, if both stars are resolved spectroscopically, accurately determined radii and masses could be obtained from the simultaneous solutions of the light and the radial velocity curves. In addition to the radii, which are not available from visual binaries, the eclipsing spectroscopic binaries provide masses, effective temperatures and the absolute dimensions of

the orbit, from which absolute brightness could be calculated. Provided with a parallax, either the physical parameters or the parallax could mutually be tested by comparing the photometric and the trigonometric distance moduli. Otherwise, a proper solution would provide not only the most reliable stellar parameters, but also a reliable photometric distance (parallax) as an independent quantity.

The critical compilations of stellar parameters and absolute dimensions of binary components were initiated, and continued with increasing quantity and quality especially by Popper (1980) and Harmanec (1988). Andersen (1991) collected accurate stellar masses and radii with uncertainties less than 2 per cent from the detached, double-lined eclipsing systems. The list contained 45 (90 stars) binaries which are all non-interacting, so that each star could be accepted as if evolved as single stars. Accuracies of 1-2 per cent were found to be significant for deeper astrophysical insight than merely improving the spectrum of masses and radii. Due to great sensitivity of other parameters, only limited amount of useful results could be extracted up to ± 5 per cent uncertainties.

Malkov (1993) announced a catalog of astrophysical parameters of binary systems containing 114 systems including all pre and out of main sequence, contact and semi-contact systems. Gorda & Svechnikov (1998) collected stellar masses and radii with accuracies better than 2-3 per cent from photometric, geometric, and absolute elements of 112 eclipsing binaries with

both components on the main sequence, for studying the mass-luminosity and mass-radius relations. Ages and metallicities for the components of 43 eclipsing binaries with lines of both components visible on the spectra were studied by Kovaleva (2001).

As the number of stars with reliable physical parameters is increasing, the studies concentrated more on the precision and accuracy. Therefore, Ibanoglu et al. (2006) did not combine 74 double-lined detached eclipsing Algols and 61 semi-detached Algols when plotting mass-radius, mass- T_{eff} , radius- T_{eff} , and mass-luminosity data. Lastennet & Valls-Gabaud (2002) compiled 60 non-interacting, well-detached systems with typical errors smaller than 2 per cent for masses and radii, while 5 per cent for the effective temperatures. The core of the sample was the large catalogue of Andersen (1991). As being satisfied with 10 per cent accuracy for the main-sequence stars, Hillenbrand & White (2004) studied dynamical mass constraints on pre-main-sequence evolutionary tracks with 148 stars, 88 are on the main-sequence, 27 are on the pre main-sequence and 33 are on the post main-sequence, where the source of data were Andersen (1991), Ribas et al. (2000) and Delfosse et al. (2000). Despite, the number of eclipsing binaries was 6330 in “the catalogue of eclipsing binaries” by Malkov et al. (2006), but Malkov (2007) was able to select only 215 stars (114 binaries) which are detached-main-sequence and double-lined eclipsing binary with uncertainties for masses, radii, $\log T_{eff}$, $\log L$, and $\log M$ were assumed to be 10, 10 per cent, 0.03, 0.03 and 0.1 mag or better respectively.

Eclipsing binaries are not only recognized with their accuracy, but also known to have larger spectrum of mass range especially towards larger masses in compared to visual binaries including *Hipparcos* detections (Malkov 2003). Improvements in observing and analysis techniques never stop, and collection of reliable light and radial velocity curve solutions continue. Recently, Torres, Andersen & Giménez (2010) updated the critical compilation of detached, double-lined eclipsing binaries with accurate masses and radii. Superseding Andersen (1991) list, this new list contains 190 stars (94 eclipsing binaries and α Cen). In order to fill the gaps in different mass ranges, further compilations on the accurate absolute dimensions of the eclipsing double lined spectroscopic binaries are inevitable.

The aim of this paper is to present our compilation of 514 stars which are from 257 detached eclipsing double-lined spectroscopic binaries (SB2) of the Milky Way. The number of stars in our list with reliable masses, spectroscopic mass ratios, orbital inclinations, radii, T_{eff} , $\log g$, and $v \sin i$ values as collected from the literature supersede similar compilations before. Selecting criteria and data collection from binaries and the descriptions of the quality of the data are given in Section 2. The H-R diagram, space distributions and how good a typical single star represented were discussed in Section 3 and finally conclusions were provided in Section 4.

2 The Catalogue

2.1 Selecting Criteria and Data Collection

The basic stellar (masses, radii, T_{eff} , $\log g$, $v \sin i$) and orbital (radial velocity amplitudes K_1 , K_2 , mass ratio q , orbital period P_{orb} , orbital inclination i , semi-major axis a , eccentricity e) parameters have been collected from the published material through literature from the simultaneous solutions of light and radial velocity curves of 257 detached eclipsing and double-lined spectroscopic binaries in our Galaxy. The collections are com-

plete by the date January 2, 2013. The strict initial criterion was first to make an eye inspection to the light and the radial velocity curves, to make sure the system is detached, and have sufficient number of observed data on both curves to assure acceptable accuracy. The systems having W UMa and β Lyr type light curves, which are known as contact and semi-contact systems respectively, were avoided. The near contact systems showing noticeable proximity effects such as ellipticity and reflection on their light curves were also avoided. Another criterion was to make sure all systems are in the Milky Way, so to avoid complexities involving extragalactic origins and to form a homogeneous sample.

If there were such systems studied more than once, that is, the light and the radial velocity curves determined and solved in various studies, the most recent solutions which include or compare to the previous solutions were preferred. We were aware of the fact that some of the chromospherically active binaries are possible to fulfill the above criteria. For example, if a detached, double-lined eclipsing binary is one of the studied chromospherically active binaries with starspots, we were keen to accept stellar parameters only if spotless clean solutions exist, in order to avoid negative contribution of starspots on the stellar parameters. Therefore, 24 binaries in the current collected sample are also contained in third edition of the catalogue of Chromospherically Active Binaries (CABs) by Eker et al. (2008).

2.2 Impact of Selecting Criteria and Observational Bias

Binaries have numerous advantages over single stars when determining basic stellar parameters, like masses, radii, effective temperatures, etc, through observations. Direct measurements of stellar radii come only from the light curve analysis of eclipsing binaries. Therefore, the first selection criterion is to require eclipses.

After many years of observational experience today for recognizing eclipsing nature of a light curve, it's always useful for the one to remember the famous debate, binary versus pulsation (Shapley 1914; Eddington 1918; Hall 1994), in the beginning of the twentieth century. Even if the one is sure, the light curve is in eclipsing nature, the light curve alone is not sufficient to extract absolute sizes of the orbit and radii of the component stars unless apparent angular size and distance of the eclipsing system is known independently. Radial velocity curves of eclipsing SB2 binaries not only could confirm consistency of eclipses but also provide the absolute size of the orbit by using the value of orbital inclination from the light curve analysis. Consequently, absolute sizes of radii could be computed from the eclipse durations and absolute size of the orbit. Therefore, for the second selection criterion, each eclipsing binary must be an SB2 system.

Eclipsing light curves and radial velocity curves of SB2, however, does not always assure basic stellar parameters (mass, radius, effective temperature, surface gravity, luminosity, etc.) as accurate as usable by the theoretical astronomers to compare and test their astrophysical theories. Therefore, complex cases associated with these two basic criteria must be removed by additional selection rules. So, the third selection criterion is established as “avoiding extragalactic systems” in order to form a homogeneous sample representing binaries in the Milky Way and in the Solar neighborhood.

Most stellar astrophysical theories start with the simplest assumptions, e.g. being single, spherical, non-rotating, non-pulsating etc. Complexities, such as mass loss, convective over-

shoot, rotation, pulsation etc were added later. Today there are many theoretical stellar evolution models (i.e. Pols et al. 1998; Demarque et al. 2004; Girardi et al. 2010; Ekstrom et al. 2012) competing. Apparently those models, which involve single stars, were tested and/or improved by comparing observational parameters mostly comes from binaries advantageous to provide most accurate data. Moreover, single star evolution becomes invalid if it is an interactive binary and experience mass transfer. Therefore, similar kinds of data from single stars are not only poor thus not useful but also not free from many severe complexities. For example, one can never be sure a single star is really single and evolved as a single. de Mink, Langer & Izzard (2011) claimed “the only unambiguous identification of true single stars is possible in detached binaries, which contain two-main sequence stars”. Therefore, for the fourth selection criterion in this study, “avoid interacting binaries known to be involving mass transfer, such as W UMa and β Lyr types”.

Near contact binaries, with strong proximity effects, still introduce complexities involving strong tidal synchronization, deformation of shapes and mutual irradiations of the component stars. So, fifth selection criterion, “avoid systems with proximity effects”, must be added.

Active solar-type stars with starspots may introduce minor but unavoidable complexity causing determined radii, relative temperatures to be less accurate. Therefore, sixth selection criterion, “avoid stellar activity, accept the spotless solutions”.

2.3 Description and Quality of the Data

The catalogue is available in an electronic format (Table 1). The content of the catalogue are organized as a table of 257 rows and 60 columns. Thus, each row of data belongs to a detached eclipsing binary, which is an SB2 system. The columns and their descriptions were given in Table 2, where one may notice the data were carefully referenced for interested readers who want to see original sources. Original sources, however, are heterogeneous to use the older and the newer values of GM_{\odot} and R_{\odot} when deriving the observed masses and radii. Since contributing uncertainty of those constants is not entirely negligible (0.23 per cent) as estimated by Torres et al. (2010), by means of their formulae, the collected masses and radii were homogenized using $GM_{\odot} = 1.3271244 \times 10^{20} \text{ m}^3\text{s}^{-2}$ (Standish 1995) and $R_{\odot} = 6.9566 \times 10^8 \text{ m}$ (Haberreiter, Schmutz & Kosovichev 2008). Next, surface gravities and luminosities recomputed from the homogenized quantities. Those re-evaluated quantities and their associated errors are listed in Table 3 where columns are self explanatory.

Containing 514 stars (257 binaries), the present catalogue supersedes the most recent collection by Torres et al. (2010) with 190 stars (94 eclipsing systems and α Cen). Both catalogues are similar in a sense containing detached eclipsing binaries with an exception that α Cen being astrometric binary is excluded. Moreover, extragalactic binary OGLE 051019, which is in the list of Torres et al. (2010), is also excluded because it is not in our Galaxy. As a result, only 93 binaries are common in both catalogues, hence there are substantial amount of excess (257-93=164) in the present catalogue. However, it is prudent to compare the quality of the data rather than a plain number. Torres et al. (2010) preferred to collect binaries with the masses and radii of both stars to be known within errors of ± 3 per cent accuracy or better. Rather than binaries, present study concentrates on component stars and collects individual stars with most accurate masses and radii. In the present sample, the number

of stars both mass and radius within ± 3 per cent accuracy or better is 311. The number implies 67 per cent more stars than Torres et al. (2010) with similar accuracy. Among the 311, the 292 stars are matched binaries, thus the number of Galactic binaries with similar accuracy increased from 93 to 146 (57 per cent) in this study. When comparing the most accurate data, that is, the number of individual stars both mass and radius with accuracies ± 1 per cent or better are 93 and 43 in the present list and in the list of Torres et al. (2010), respectively. Such improvements justify the publication of the present catalogue.

Among the 93 binaries which are common between the present catalogue and the catalogue of Torres et al. (2010), only one binary, EW Ori, has been re-studied later by Clausen et al. (2010). Thus, 92 binaries in both catalogues have common references from which catalogue parameters were taken. Therefore, catalogue values and accuracies must be similar. Nevertheless, we have noticed few small negligible differences most probably originating from the preferences among the multiple references. Additionally, few limited non-negligible differences exist because of identifying the primary and the secondary, which will be explained below while discussing the mass ratio (q) distribution of the present sample.

Statistics of masses, radii, effective temperatures, surface gravities, luminosity of individual stars, and orbital semi-major axis (a), mass ratio of binaries in the present sample are summarized in Table 4. Maximum and minimum values of those data with the identified star or the system are given in the first four rows. Following are mean, mode and median values. Maximum, minimum, mean, mode and median values of the associated errors are given in the last five lines. Relative errors are indicated by % sign after the value, otherwise the errors are absolute. Being related with characteristics of the present sample, some of the distributions will be discussed below.

2.3.1 Apparent Magnitude and Period Distributions

Apparent magnitude distribution of the present sample (257 systems) is shown in Fig. 1. Large range of apparent magnitudes from very bright (1.89 mag, β Aur) to dimmest (19.92 mag, SDSS-MEB-1) display a peak at $V = 9$ mag, thus most of the systems are contained at 8, 9 or 10 magnitudes.

The orbital period of the sample covers a range from $P_{orb} = 0.30$ days (DV Psc) to $P_{orb} = 99.7638$ days (V379 Cep). The distribution on the logarithmic scale is displayed in Fig. 2. Accordingly, the most common orbital periods are close to 2.5 days. For a given mass, bigger orbital periods mean larger orbital sizes. Larger orbital size, however, decreases the probability of having eclipses. Since, our sample contains only eclipsing binaries, the decrease towards longer periods in Fig. 2 is clear and it must be effected by the probability of eclipses. Researchers prefer to study short period systems because they are easier to observe. This is an additional bias to increase the number of systems towards the short periods. However, according to Fig. 2, starting from $\log P_{orb}$ (days) = 0.4, the number of systems decreases quickly towards the short periods. This could be explained by the fact that decreasing orbital period means decreasing the orbital sizes. Decreasing orbital size, however, increases the proximity effects such as, reflection and deviation from spherical shapes. Avoiding systems with proximity effects must be the main cause of the decrease towards short periods starting from the peak period $P_{orb} = 2.5$ days.

Distribution of orbital periods among the spectral types (pri-

mary components) is given in Table 5. Shortest orbital periods (0.30 to 0.63 days) could be found among F and later spectral types. Such small orbital periods does not exist for the binaries with spectral types O, B and A. The system with the smallest orbital period ($P_{orb} = 0.30$ days, DV Psc) has components of spectral types K4V+M1V (Zhang & Zhang 2007).

Among the O-type binaries, the shortest orbital period is 1.62 days which belongs to V1182 Aql (Mayer et al. 2005), while the longest orbital period is only 4.24 days for V1292 Sco (Sana et al. 2006). It appears odd to find the maximum orbital period of O-type systems as short as 4.24 days. The long period cut off for the B-type systems is at 99.76 days which is the orbital period of V379 Cep (Harmanec et al. 2007). Normally, larger radii would increase the probability of eclipses, thus, one would expect to see more O-type systems thus the median values of the orbital periods (Table 5) must increase towards earliest spectral types. However, the median $\log P_{orb}$ decrease from G-type to O-type. Moreover, according to Table 5 (column 9), there are 247 binaries from B to M types. Consequently, 8 out of 247 with $\log P_{orb}$ (days) > 1.4 , and 32 out of 247 with $\log P_{orb} > 1$ hence, probability to have chance 0 out of 10, which is the case for O-type systems, is 0.72 ($\log P_{orb}$ (days) > 1.4) and 0.25 ($\log P_{orb}$ (days) > 1) not compellingly low. These numbers might be biased somehow to very high values, but even computing only on the B-type stars (disadvantage of smaller subset), 1 out of 52 and 8 out of 52 gives probabilities of 0.82 ($\log P_{orb}$ (days) > 1.4) and 0.19 ($\log P_{orb}$ (days) > 1) to have no O-type stars at longer periods. The apparent lack of O-type stars at longer periods suffers from statistical significance because of the small size of this subset. However, inspecting the median values of mass ratios (Table 5), one may notice that the median values of mass ratio (q), is almost constant (median $q=0.92$) for late spectral types (G, K, M), but it decreases from F-types to O-types as low as median $q = 0.708$. This implies that, O-types stars have higher probability to have a secondary with less massive than the primary. Combining this with faster rotation, the odds of detecting the secondary due to rotational broadening increases. Thus, faster rotation of O-type stars appears to be the main reason finding them with the least number and smallest upper cut off for the orbital periods on the Table 5.

2.3.2 Masses and Radii

The distributions of masses and radii of 514 stars are shown in Fig. 3. Similar appearance of both distributions is not a coincidence. This is because, almost all of the stars of the present sample are on the main sequence, only a few exceptions e.g. BW Aqr, V379 Cep, RT CrB, TZ For, AI Hya, V1292 Sco appear to have evolved components. Similar appearance of the two distributions, thus, imply a strong relation between stellar masses and radii, that the shape of both distributions is almost identical.

The uncertainty distributions of masses and radii are displayed in Fig. 4. Fig 4a, c are in the accumulated form and Fig. 4b, d are ordinary histogram showing the number of stars in 1 per cent bin up to 20 percent uncertainty. Fig. 4a, c indicate that in the sample there are 193 stars with masses better than 1 per cent, 390 stars with masses better than 3 per cent, and 443 stars with masses better than 5 per cent uncertainties. Regarding to radii in the sample, there are 158 stars with radii better than 1 per cent, 379 stars with radii better than 3 per cent, and 437 stars with radii better than 5 per cent uncertainties. The uncertainty range up to 20 per cent includes all mass data, while the radii data contain 98 per cent of sample stars in the same

range. That is, there are only nine stars with uncertainties larger than 20 per cent in radius.

2.3.3 Mass Ratio and Spectral Types

The spectroscopic mass ratio (q) of the components is one of the most fundamental parameter of binary systems. It is conventionally defined as mass of the secondary divided by the mass of the primary. If the secondary is the less massive component, q is always less than one. Here, the light curve approaches are adopted; the primary is the eclipsed star during the primary minimum which is the deeper one of the two minima. Consequently, all mass ratios are determined spectroscopically from the radial velocity amplitudes as K_1/K_2 .

The mass ratio distribution of the sample stars is displayed in Fig. 5. The most common mass ratio of the sample is close to 0.9 and it is distributed within the range 0.2 to 1.2. The values $q < 1$ indicate more massive hotter primary and a cooler less massive secondary. This is the case for young unevolved binaries on the main sequence. On the other hand, the values $q > 1$ implies evolved pairs that more massive component cooler than the less massive secondary. Even when there would be no evolved pairs, some empirical mass ratios above unity expected because of less precise systems with a q near unity. According to Fig. 5, there are 21 systems with $q > 1$. Examining their positions on the H-R diagram, seven systems (TZ For, V1130 Tau, AI Hya, GZ Leo, RT CrB, V2368 Oph, V885 Cyg) were found for sure to have evolved cooler components. The rest have some ambiguity because one can not identify the primary and the secondary due to component masses and/or temperatures so close.

Using published spectral types (Table 1) and counting each component as a single star, spectral type distribution of 514 stars (257 pairs) is shown in Fig. 6. Except for O-types, there exist sufficient number of stars at all spectral types. The most crowded spectral types are F, A and B. So, with an abrupt increase at B, number of stars increase until F, then there is a considerable sudden decrease to G then gradual decrease towards M. Readers should be aware of that the papers announcing those spectral types (Table 1) use different kinds of estimates, from professional MK(K) types to very rough estimates, even from photometric indices.

The hottest star in the sample has an effective temperature 43000K which is the O-type primary of V1182 Aql (Mayer et al. 2005), while the coldest star in the sample has an effective temperature 2750K which is M-type secondary of KIC10935310 (Çakırlı, İbanoğlu 2013).

3 Discussion

3.1 H-R diagram

The H-R diagram is a primary tool to demonstrate and study stellar evolution. Representing the stars with most accurate mass and radius, the present sample on the H-R diagram has been investigated. Taking the effective temperatures ($\log T_{eff}$) from the catalogue (Table 1) and using the homogenized luminosities ($\log L_{\odot}$) from Table 3, the positions of 472 (236 binaries) stars on the H-R diagram are shown in Fig. 7. Theoretical stellar evolution lines (from Pols et al. 1998), ZAMS and TAMS are drawn to indicate evolutionary status of the current sample. Almost the entire sample appears to be within the main-sequence

band. Evidently, there are no supergiants despite the selection criteria do not imply such a result directly. Considering the fact that evolved stars could be observed at larger distances than their main-sequence counterparts and the probability of having eclipses is higher if the radii of the components are larger, the absence of giants and supergiants in the present sample needs to be explained. Smaller number of evolved stars, which is a consequence of shorter lifetime of evolved phases, and low probability of evolving both components to the sizes comparable to each other, which permits the detection of eclipses, must be more effective than the eclipse favoring conditions. Obviously, much smaller size of companion stars if exists, and/or huge difference of brightness between the components leave out some giants and supergiants to be detected as SB2 eclipsing binaries.

Although there are 514 stars (257 binaries) in the present sample, we are able to place 472 stars (236 binaries) with effective temperatures on the H-R diagram. This is because the catalogue (Table 1) has 21 systems (42 stars have no published temperatures; see Table 1) without temperatures. When solving the light and the radial velocity curves, some authors, who are not trusting stellar temperature determinations, are satisfied with the temperature ratios rather than absolute temperatures (i.e. Helminiak et al. 2009). The obtained masses and radii for those 21 systems are still reliable. Therefore, they were included in the catalogue.

Sample stars on H-R diagram were displayed as four sub-samples according to accuracy limits. The four sub-samples [both mass and radius up to ± 1 per cent accuracy 91 stars, between ± 1 to ± 3 per cent (211 stars), between ± 3 to ± 5 per cent (71 stars) and worse than ± 5 per cent (99 stars)] were shown in Fig. 7a with different symbols in order to investigate if there are any preferred positions among the data of different class of accuracy. Except for the most accurate sub-sample (91 stars) which covers a spectral range from A0 to M3 corresponding to a temperature range 10000 K to 3000 K, the other sub samples have full ranges covering spectral types from O5 to M3 and temperatures from 43000 K to 3000 K. Preference of certain locations by certain sub-samples cannot be noticed except the most accurate sub-sample. All other sub-samples appear to be evenly distributed along the main-sequence band.

In order to investigate accuracy and precision of the positions on the H-R diagram (Fig. 7), the published uncertainties of radii and temperatures have been propagated to estimate the uncertainty of the luminosities. Among the 472 stars (236 binaries) plotted on Fig. 7a, the seven systems (2MASS J01542930+0053266, 2MASS J16502074+4639013 and 2MASS J19071662+4639532, GZ Leo, HY Vir, δ Vel, V415 Aql) do not have published uncertainties for their temperatures and seven systems (V467 Vel, IQ Aqr, SZ Cam, RX Her, V2083 Cyg, MR Del, AE For) were found to have uncertainty of temperatures only for their secondaries. Leaving the systems without any temperature uncertainty out, and assigning same uncertainty to the primary temperature for those having only uncertainty for the secondary temperatures, the relative uncertainties of luminosities for 458 stars (229 binaries) were computed by the method of error propagation. All computed uncertainties are less than 51 per cent except for one star, which is the secondary of V1292 Sco. The 18.8 per cent uncertainty of the temperature and 51.9 per cent uncertainty on the radius propagate to be 128 per cent for the luminosity for this star. Among 458 stars, 87.6 per cent (401 stars) have relative errors less than 20 per cent. The rest, 57 stars are placed on the H-R diagram with their error bars (Fig. 7b) in order to investigate if certain locations are preferred by

the stars with the biggest error bars. Evenly distribution along the main-sequence band covering the full range of spectral types is clear. However, one must remember that the most accurate sub-sample (91 stars) does not mean to have the most accurate positions on the H-R diagram because an uncertainty at an effective temperature contributes at both axes. Consequently there are contributions from all subsamples to Fig. 7b. Nevertheless, it is interesting to notice the least accurate sub-sample dominates (44 per cent) although it occupies only 21 per cent (99 stars) among 472 stars in Fig. 7a. The contributions to Fig. 7b from the other three sub-samples are 5, 18, and 9, which sum up to be 56 per cent, respectively from the groups of 91, 211 and 71 stars of the most accurate and the other two subsamples in Fig. 7a.

Determination of observed temperatures appears to be the biggest obstacle of observational astrophysics to study stellar evolution on the H-R diagram. Considering the fact that, some authors prefer to publish internal errors, which could be unrealistically small, e.g. the effective temperatures of AE For $T_{eff}(pri)=4100\pm 6$ K and $T_{eff}(sec)=4055\pm 6$ K (Rozyczka et al. 2013), XY UMa $T_{eff}(pri)=5200\pm 7$ K and $T_{eff}(sec)=4125\pm 7$ K (Pribulla et al. 2001), and DV Psc $T_{eff}(pri)=4450\pm 8$ K and $T_{eff}(sec)=3614\pm 8$ K (Zhang & Zhang 2007), many of the uncertainties on the effective temperatures of the present sample are optimistic. But still, the present sample has the most accurate stellar positions on the H-R diagram ever been obtained from the simultaneous solutions of light and radial velocity curves of detached eclipsing binaries and the stellar parameters would be the most reliable, thus, empirical relations and astrophysical theories could be tested.

3.2 Space Distributions

Distributions of the present sample on the equatorial and the Galactic coordinates are displayed in Fig. 8. Although 257 systems appear to be homogeneously distributed, a significant asymmetry between northern and southern hemispheres is indicated by the numbers in the lower right corner of Fig. 8a. There exist 168 northern binaries with positive declinations ($\delta \geq 0^\circ$), while there are nearly half number of binaries in the southern hemisphere, that is, 89 systems with negative declination ($\delta < 0^\circ$). Detailed analyses is not in the scope of the present paper, but in the first approximation, the excess in the northern hemisphere could be explained by overpopulation of the northern telescopes and/or astronomers to the southern ones. A perceptible concentration of stars towards the Galactic plane is noticeable even on the equatorial coordinates that the Galactic plane drawn on Fig. 8a, where the Galactic center is marked by a star symbol.

Although a negligible north-south asymmetry is indicated by the numbers at the lower left corner, nearly symmetric distribution with respect to Galactic plane was shown on Fig. 8b. It is also noticeable that there are regions on the Galactic plane where the stars appear to be grouping towards the Galactic longitudes 30, 70 and 110 degrees. These are the directions associated with the local arms structure of our Galaxy. On the other hand, less populated, “empty region” towards $l = 250$, $b = -45$ degrees are also noticeable on the Fig. 8b.

Among the 257 systems in the present sample, 205 systems were found to have distances published at articles from where catalogue data were taken. Therefore, we had to search extra sources for the distances of 52 systems, where 24 of them were found to have *Hipparcos* parallaxes (van Leeuwen 2007). For the

rest with no trigonometric parallaxes, the formulae by Bilir et al. (2008a), was used in estimating distances. Finally, the distance distribution of the sample in the Solar neighborhood were presented in Fig. 9. The Fig. 9b indicates the number of systems within each incremental 200 pc bins. Accumulated form of the same data (Fig. 9a) indicates that 90 per cent of sample stars are contained within 1 kpc from the Sun, where the rest are located at distances up to 4.6 kpc. Such distances are far more than the detection limit of *Hipparcos* (Perryman et al. 1997). In fact, excluding the parallaxes with large relative errors (e.g. $\sigma_\pi/\pi > 0.5$) in the sample, there are 119 systems (46.3 per cent) with reliable parallaxes, thus, more than half (53.7 per cent) of the sample had to rely on the photometric distances. Compared to other field stars, the present sample are advantageous to provide the most accurate photometric distances together with physical parameters.

Figure 10 displays space distribution of the sample in the Solar neighbourhood on the Galactic plane (X - Y), where X is towards the Galactic center and Y is towards the Galactic rotation. With a median distance of 1528 pc, O-type binaries are the most distant objects. Closest one is SZ Cam which is 870 pc away (Tamajo et al. 2012), the most distant one is DH Cep with 2767 pc (Hilditch et al. 1996). There exist 10 binaries with O-type primary in the present sample. The distant stars, mostly O-B type binaries on the X - Y plane were interesting (Fig. 10a) as if to imply one of the local Galactic arms. Indeed, after plotting, O-type binaries in our sample on Fig. 11, which shows Galactic arm structure by Xu et al. (2009), the position of O-type binaries and the Sun on the Galactic plane became clear. The present sample is mostly located within 1 kpc in the Solar neighborhood which is itself positioned between the two local arms Carina-Sagittarius and Orion Spur. The Orion spur itself situated between the Perseus and Carina-Sagittarius arms.

Figure 10b shows distribution perpendicular to the Galactic plane, where the scaleheight of the thin disc ($H = 220$ pc) according to Bilir et al. (2006a,b, 2008b). Distant systems, mostly with O-B type binaries on the Galactic plane are distinguishable from the concentrated central region.

On a closer look, the space distribution of the concentrated region was shown in Fig. 12. Unlike large scale appearance, the very central region within 300 pc could be described evenly spread over the space. Nevertheless, even in this closer look the local Galactic disc structure is noticeable when the scaleheight lines were drawn on Fig. 12b. One may easily notice that all local binaries ($d \leq 300$ pc) are contained within the thin-disc scaleheight limit except for only three systems.

3.3 How Good Single Stars were Represented?

The components of close binary systems with proximity effects are flattened at various degrees by fast rotation and tidally elongated towards each other by the mutual gravity in addition to irradiation effects. All these effects may be negligible in the case of detached binaries, where single star evolution could be applied to each component in better approximation. It is advantageous to know how good the present sample represents non-rotating spherical single stars of a given mass. However, the flattening due to rotation, the mass loss due to stellar winds may not be ignorable even for the case of single stars.

The tidal evolution forces the components of close binaries into tidal synchronization. For interested readers, the catalogue contains projected rotational velocities ($v \sin i$), from which one

can compute if tidal synchronization was achieved. More importantly, rotation and Roche lobe filling ratio are two indicators for the component stars deviating from sphericity. For the sake of confidence, the sphericity of the present sample was inspected by computing the Roche model of each binary.

Mass, mass ratio and orbital period determine the sizes and the shapes of the Roche lobes (Kopal 1978). Classical definition of close (interacting) binary systems was given as $R_1 + R_2 \geq 0.1a$, where a is the semi-major axis of the orbit and $R_{1,2}$ are the radii of the components, the subscripts are for the primary and the secondary. With counter definition $R_1 + R_2 < 0.1a$, the non-interacting binaries, however, are all well detached systems definitely far from proximity effects and well contained in the Roche lobes that their shapes are believed to be spherical. Unfortunately, the number of such systems is only 24 in the present sample and much less in previous samples (four in the list of Torres et al. 2010). In order to increase the number of detached systems, one prefers to loosen the condition $R_1 + R_2 < 0.1a$.

Equipotential surface of a component star is represented by four fractional radii defined as: $r(\text{side})$, $r(\text{back})$, $r(\text{point})$ and $r(\text{pole})$. The smallest of those is the $r(\text{pole})$ and the largest one is the $r(\text{point})$. The difference between those fractional radii increases by increasing filling ratio. In order to test and establish a well-structured limit for deviation from the sphericity we have computed Roche model of the sample binaries using Binary Maker¹. This allowed us to compare fractional radii and made eye inspection of the shapes of the component.

Figure 13 displays how radii and shapes of the components change with respect to the Roche lobes from 60 per cent filling to the higher rates of filling factors (FF), which is defined as $FF = \bar{r}/\bar{r}_{RL}$, where, \bar{r} is average radius, \bar{r}_{RL} is Roche-lobe radius relative to the semi-major axis. It can be deduced from an eye inspection that deviations from sphericity could be ignorable for small filling factors which can be up to 75 per cent, a value corresponding to the difference between the $r(\text{side})$ and the $r(\text{pole})$ being less than 1 per cent. By the way, the difference between the $r(\text{point})$ and the $r(\text{side})$ being larger than 1 per cent indicate tidal elongation and tidal synchronization when $P_{rot} = P_{orb}$. By a careful look, eye could feel larger deviations (deviation > 1 per cent corresponding $FF > 75$ per cent), thus, non-spherical shapes of the component stars of V478 Cyg and DH Cep on Fig. 13 are noticeable. On the other hand, with less filling factors ($FF < 75$ per cent), component stars of AG Ari and V760 Sco appear spherical.

The distribution of the filling ratios of the component stars in the present sample is displayed in Fig. 14. Accordingly, 426 stars (82.9 per cent of the sample) have filling factors less than 70 per cent, which could be assumed to have spherical shapes. If one could expand sphericity limit to 75 per cent filling factor, the number of spherical stars increases to 455 (88.5 per cent of the sample). Overall, 20 binaries were found as both components exceed the limit of 75 per cent filling factor, which includes seven O-type binaries. The number of binaries at least one component exceeding the limit is 39, which includes nine O-type binaries. That is, among the 39 there are 19 systems only one component is spherical. We first tempted to discard the systems with non-spherical components. However, the number of O-type binaries is only 10 (3.9 per cent of the sample). Among the 10, only one (Y Cyg, with $P_{orb} = 2.996$ days) were found to have both components with spherical shapes. Therefore, we have decided not to discard the systems with more than 75 per cent filling factor

¹<http://www.binarymaker.com/>

and left this choice to researchers, who may alter sphericity limit according to their specific needs.

4 Conclusions

- The most accurate stellar parameters (masses, radii, temperatures, surface gravities, luminosities, projected rotational velocities, radial velocity amplitudes, mass ratio, orbital period, orbital inclination, semi-major axis, eccentricity) were compiled from the simultaneous solutions of light and radial velocity curves of detached double-lined eclipsing binaries.
- The masses and radii were homogenized using most recent values of $GM_{\odot} = 1.3271244 \times 10^{20} \text{ m}^3\text{s}^{-2}$ (Standish 1995) and $R_{\odot} = 6.9566 \times 10^8 \text{ m}$ (Haberreiter et al. 2008). Surface gravities and luminosities recomputed using homogenized masses and radii.
- Apparent magnitudes, orbital periods, masses, radii, mass ratios, spectral types and space distribution of the present sample were discussed.
- The number of stars with both mass and radius as accurate as 1 per cent is 93, as accurate as 3 per cent is 311, and as accurate as 5 per cent is 388.
- Filling ratios of the current sample were studied. Thus, the geometrical shapes of the component stars were determined. Up to 75 per cent of filling factors, stars are found almost spherical within 1 per cent uncertainty.
- Giants and supergiants are missing in the present sample. Observational astronomers are encouraged to explore eclipsing binaries among giants and supergiants. Improving light curve observing techniques for discovering small amplitude SB2 eclipsing systems is a challenge

5 Acknowledgments

This work has been supported in part by the Scientific and Technological Research Council of Turkey (TÜBİTAK) grant numbers 106T688 and 111T224. Authors would like to thank anonymous referee who provided valuable comments for improving the manuscript and Mr. Muzaffer Karasulu for proof reading. This research has made use of the SIMBAD database, operated at CDS, Strasbourg, France and NASA's Astrophysics Data System. We would like to thank Dr. Nilda Oklay for helping online material.

References

- Andersen J., 1991, *A&ARv*, 3, 91
- Bilir S., Karaali S., Ak S., Yaz E., Hamzaoglu E., 2006a, *NewA*, 12, 234
- Bilir S., Karaali S., Gilmore G., 2006b, *MNRAS*, 366, 1295
- Bilir S., et al., 2008a, *AN*, 329, 835
- Bilir S., Cabrera-Lavers A., Karaali S., Ak S., Yaz E., López-Corredoira M., 2008b, *PASA*, 25, 69
- Çakırlı Ö., İbanoğlu C., Sipahi E., 2013, *MNRAS*, 429, 85
- Clausen J. V., Bruntt H., Olsen E. H., Helt B. E., Claret A., 2010, *A&A*, 511A, 22
- Delfosse X., Forveille T., Ségransan D., Beuzit J.-L., Udry S., Perrier C., Mayor M., 2000, *A&A*, 364, 217
- de Mink S. E., Langer N., Izzard R. G., 2011, *Societe Royale des Sciences de Liege Bulletin*, 80, 543
- Demarque, P., Woo, J., Kim, Y., Yi, S.K., 2004, *ApJS*, 155, 667
- Duquenooy A., Mayor M., 1991, *A&A*, 248, 485
- Eddington, A. S., 1918, *MNRAS*, 79, 2
- Eker Z., et al., 2008, *MNRAS*, 389, 1722
- Ekstrom, S., et al., 2012, *A&A*, 537A, 146
- Girardi, L., et al., 2010, *ApJ*, 724, 1030
- Gorda S. Y., Svechnikov M. A., 1998, *ARep*, 42, 793
- Haberreiter M., Schmutz W., Kosovichev A. G., 2008, *ApJ*, 675L, 53
- Hall D. S., 1994, *International Amateur-Professional Photoelectric Photometry Communication*, No. 54, 1
- Harmanec P., 1988, *BAICz*, 39, 329
- Harmanec P., et al., 2007, *A&A*, 463, 1061
- Helminiak K. G., Konacki M., Ratajczak M., Muterspaugh M. W., 2009, *MNRAS*, 400, 969
- Hilditch R. W., Harries T. J., Bell S. A., 1996, *A&A*, 314, 165
- Hillenbrand L. A., White R. J., 2004, *ApJ*, 604, 741
- Ibanoğlu C., Soydugan F., Soydugan E., Dervişoğlu A., 2006, *MNRAS*, 373, 435
- Kovaleva D. A., 2001, *ARep*, 45, 972
- Kopal Z., 1978, *Dynamics of close binary systems*, Dordrecht, D. Reidel Publishing Co. (Astrophysics and Space Science Library. Volume 68)
- Lastennet E., Valls-Gabaud D., 2002, *A&A*, 396, 551
- Malkov O. Y., 1993, *BICDS*, 42, 27
- Malkov O. Y., 2003, *A&A*, 402, 1055
- Malkov O. Y., Oblak E., Snegireva E. A., Torra J., 2006, *A&A*, 446, 785
- Malkov O. Y., 2007, *MNRAS*, 382, 1073
- Mayer P., Drechsel H., Lorenz R., 2005, *ApJS*, 161, 171
- Perryman M. A. C., et al., 1997, *A&A*, 323L, 49
- Pols O. R., Schröder K.-P., Hurley J. R., Tout C. A., Eggleton P. P., 1998, *MNRAS*, 298, 525
- Popper D. M., 1980, *ARA&A*, 18, 115
- Pribulla T., Chochol D., Heckert P. A., Errico L., Vittone A. A., Parimucha Š., Teodorani M., 2001, *A&A*, 371, 997

- Rozyczka M., Pietrukowicz P., Kaluzny J., Pych W., Angeloni R., Dékány I., 2013, *MNRAS*, 429, 1840
- Ribas I., Jordi C., Torra J., Giménez Á., 2000, *MNRAS*, 313, 99
- Sana H., Gosset E., Rauw G., 2006, *MNRAS*, 371, 67
- Shapley H., 1914, *ApJ*, 40, 448
- Standish E. M., 1995, *Highlights of Astronomy*, 10, 180
- Tamajo E., Munari U., Siviero A., Tomasella L., Dallaporta S., 2012, *A&A*, 539A, 139
- Torres G., Andersen J., Giménez A., 2010, *A&ARv*, 18, 67
- van Leeuwen F., 2007, *A&A*, 474, 653
- Xu Y., Voronkov M. A., Pandian J. D., Li J. J., Sobolev A. M., Brunthaler A., Ritter B., Menten K. M., 2009, *A&A*, 507, 1117
- Zhang X. B., Zhang R. X., 2007, *MNRAS*, 382, 1133

Table 2: Column descriptions of the catalogue data.

Column	Description	Remark
1	ID	Order number
2	Star name	The most common name
3	HD	Henry Draper catalogue number
4	Hip	<i>Hipparcos</i> catalogue number
5	SAO	Smithsonian Astrophysical Observatory star catalogue number
6	α (hh:mm:ss.ss)	Right ascension in J2000
7	δ (dd:mm:ss.ss)	Declination in J2000
8	l (deg)	Galactic longitude
9	b (deg)	Galactic latitude
10	Spt Type	Spectral types of components
11	Ref	Reference to spectral types
12	V (mag)	Johnson V apparent magnitude of system
13	π (mas)	Trigonometric parallax
14	σ_π (mas)	Standard error of π
15	Ref	Reference to π and σ_π
16	γ (kms ⁻¹)	Center of mass velocity of orbit
17	σ_γ (kms ⁻¹)	Standard error of γ
18	Ref	Reference to γ
19	K_1 (kms ⁻¹)	Radial velocity amplitude of primary
20	σ_{K_1} (kms ⁻¹)	Standard error of K_1
21	K_2 (kms ⁻¹)	Radial velocity amplitude of secondary
22	σ_{K_2} (kms ⁻¹)	Standard error of K_2
23	q	Mass ratio of components
24	Ref	Reference to q
25	P_{orb} (day)	Orbital period
26	Ref	Reference to P
27	a (R_\odot)	Semi-major axis of orbit
28	σ_a (R_\odot)	Standard error of a
29	i (deg)	Orbital inclination
30	e	Orbital eccentricity
31	Ref	Reference to a , e , i
32	FF1 (%)	Roche lobe filling ratio of primary
33	FF2 (%)	Roche lobe filling ratio of secondary
34	M_1 (M_\odot)	Mass of primary
35	σ_{M_1} (M_\odot)	Standard error of M_1
36	M_2 (M_\odot)	Mass of secondary
37	σ_{M_2} (M_\odot)	Standard error of M_2
38	R_1 (R_\odot)	Radius of primary
39	σ_{R_1} (R_\odot)	Standard error of R_1
40	R_2 (R_\odot)	Radius of secondary
41	σ_{R_2} (R_\odot)	Standard error of R_2
42	Ref	References to M_1 , M_2 , R_1 and R_2
43	T_1 (K)	Effective temperature of primary
44	σ_{T_1} (K)	Standard error of T_1
45	T_2 (K)	Effective temperature of secondary
46	σ_{T_2} (K)	Standard error of T_2
47	Ref	References to T_1 and T_2
48	$\log g_1$ (cms ⁻²)	Surface gravity on primary
49	$\sigma_{\log g_1}$ (cms ⁻²)	Standard error of $\log g_1$
50	$\log g_2$ (cms ⁻²)	Surface gravity on secondary
51	$\sigma_{\log g_2}$ (cms ⁻²)	Standard error of $\log g_2$
52	Ref	References to $\log g_1$ and $\log g_2$
53	$v_1 \sin i$ (kms ⁻¹)	Projected equatorial rotational velocity of primary
54	$\sigma_{v_1 \sin i}$ (kms ⁻¹)	Standard error of $v_1 \sin i$
55	$v_2 \sin i$ (kms ⁻¹)	Projected equatorial rotational velocity of secondary
56	$\sigma_{v_2 \sin i}$ (kms ⁻¹)	Standard error of $v_2 \sin i$
57	Ref	Reference to $v_1 \sin i$ and $v_2 \sin i$
58	d (pc)	Distance of binary
59	σ_d (pc)	Standard error of distance
60	Ref	Reference to the distance

Table 3: cont.

ID System	M_1 (M/M_{\odot})	M_2 (M/M_{\odot})	R_1 (R/R_{\odot})	R_2 (R/R_{\odot})	T_1 (K)	T_2 (K)	$\log L_1$ (L/L_{\odot})	$\log L_2$ (L/L_{\odot})	$\log g_1$ (cgs)	$\log g_2$ (cgs)	a (R_{\odot})
241 AH Cep	15.565±0.202	13.714±0.202	6.385±0.110	5.864±0.130	29900±1000	28600±1000	4.466±0.065	4.315±0.069	4.020±0.016	4.039±0.021	19.014±0.140
242 V364 Lac	2.334±0.015	2.296±0.025	3.308±0.038	2.986±0.035	8250±150	8500±150	1.658±0.034	1.621±0.034	3.767±0.010	3.849±0.011	26.519±0.080
243 V453 Cep	2.575±0.050	2.478±0.050	2.112±0.201	2.011±0.201	10300±500	10400±500	1.654±0.138	1.628±0.141	4.200±0.092	4.225±0.097	8.086±0.060
244 NY Cep	13.152±1.012	9.323±1.036	6.843±0.704	5.434±0.503	28500±1000	23100±1000	4.443±0.124	3.878±0.127	3.887±0.108	3.937±0.106	73.119±2.435
245 EF Aqr	1.244±0.008	0.946±0.006	1.338±0.012	0.956±0.012	6150±65	5185±110	0.362±0.020	-0.227±0.040	4.280±0.008	4.453±0.011	10.996±0.020
246 CW Cep	11.797±0.140	11.067±0.140	5.524±0.121	5.030±0.121	28300±1000	27700±1000	4.245±0.070	4.126±0.072	4.025±0.020	4.079±0.022	23.326±0.081
247 PV Cas	2.757±0.049	2.816±0.061	2.298±0.021	2.257±0.016	10200±250	10200±250	1.710±0.046	1.695±0.045	4.156±0.011	4.181±0.011	10.837±0.040
248 RT And	1.240±0.030	0.907±0.020	1.268±0.015	0.906±0.013	6095±214	4732±110	0.299±0.067	-0.432±0.044	4.325±0.015	4.481±0.016	3.986
249 V396 Cas	2.397±0.022	1.901±0.016	2.592±0.013	1.779±0.010	9225±150	8550±120	1.640±0.030	1.181±0.026	3.991±0.006	4.217±0.006	21.334±0.110
250 2MASS J23143816+0339493	0.469±0.002	0.383±0.001	0.441±0.002	0.374±0.002	3460±180	3320±180	-1.602±0.101	-1.817±0.106	4.820±0.004	4.876±0.005	5.733±0.020
251 NSVS 11868841	0.870±0.074	0.607±0.053	0.985±0.030	0.903±0.026	5250±135	5020±135	-0.179±0.055	-0.333±0.057	4.391±0.048	4.310±0.048	3.417±0.100
252 AR Cas	5.902±0.200	1.869±0.060	5.064±0.060	1.604±0.030	17200±500	8150±200	3.304±0.055	1.008±0.048	3.800±0.018	4.299±0.022	27.727±0.993
253 V731 Cep	2.577±0.098	2.017±0.084	1.823±0.030	1.717±0.025	10700±200	9265±220	1.592±0.037	1.290±0.045	4.328±0.022	4.273±0.023	23.276±0.290
254 IT Cas	1.330±0.009	1.328±0.008	1.603±0.015	1.569±0.040	6470±110	6470±110	0.607±0.032	0.588±0.039	4.152±0.009	4.170±0.023	14.436±0.040
255 BK Peg	1.414±0.007	1.257±0.005	1.985±0.008	1.472±0.017	6265±85	6320±30	0.736±0.025	0.492±0.013	3.993±0.004	4.202±0.010	18.173±0.200
256 AL Scl	3.617±0.110	1.703±0.040	3.241±0.050	1.401±0.020	13550±350	10300±360	2.502±0.050	1.297±0.067	3.975±0.019	4.376±0.016	13.335±0.150
257 V821 Cas	1.996±0.166	1.597±0.187	2.296±0.109	1.382±0.119	9400±400	8450±380	1.568±0.094	0.942±0.124	4.016±0.059	4.360±0.101	9.432±0.010

Table 4: Summary statistics of the present sample.

	Mass (M/M_{\odot})	Radius (R/R_{\odot})	T_{eff} (K)	$\log g$ (cms^{-2})	Luminosity (L/L_{\odot})	a (R_{\odot})	q
Maximum	32.60	21.19	43000	5.077	5.554	233.25	1.114
Star (or system)	(1)	(2)	(3)	(4)	(1)	(5)	(6)
Minimum	0.18	0.21	2750	2.906	-2.553	1.85	0.237
Star (or system)	(7)	(8)	(9)	(10)	(8)	(11)	(12)
Mean	2.9	2.1	9500	4.20	2.8	18.9	0.851
Mode	1.3	1.3	6500	4.25	4.4	10.5	0.975
Median	1.5	1.7	6800	4.21	3.9	14.1	0.905
Errors							
Minimum	0.09%	0.19%	6	0.003	0.5%	0.01%	0.001
Maximum	16.8%	51.9%	4100	1.934	51%	8.54%	0.178
Mean	2.4%	3.2%	282	0.044	12.5%	0.44%	0.001
Mode	1.1%	0.9%	125	0.010	9%	0.02%	0.004
Median	1.3%	1.5%	150	0.016	10.1%	0.86%	0.007

(1) Primary of DH Cep; (2) primary of V1765 Cyg; (3) primary of V1182 Aql; (4) secondary of 2MASS J04463285+1901432; (5) V379 Cep; (6) V885 Cyg; (7) secondary of NSVS 07394765; (8) secondary of 2MASS J04463285+1901432; (9) secondary of KIC 10935310; (10) secondary of TZ For; (11) SDSS-MEB-1; (12) TYC3121-1659-1.

Table 5: Distribution of orbital periods among the spectral types of the primary components.

Spectral Type	O	B	A	F	G	K	M	Total
$-0.6 \leq \log P_{orb} < -0.2$				1	3	5	5	14
$-0.2 \leq \log P_{orb} < 0.2$		5	3	9	7	6	7	37
$0.2 \leq \log P_{orb} < 0.6$	9	28	28	21	6	6	7	105
$0.6 \leq \log P_{orb} < 1.0$	1	11	16	25	12	3	1	69
$1.0 \leq \log P_{orb} < 1.4$		7	7	5	5			24
$1.4 \leq \log P_{orb} < 1.8$			3	1	1		1	6
$1.8 \leq \log P_{orb} < 2.2$		1		1				2
Total	10	52	57	63	34	20	21	257
Median $\log P_{orb}$	0.44	0.43	0.53	0.60	0.67	0.18	0.18	
Median q	0.708	0.830	0.909	0.931	0.922	0.926	0.922	

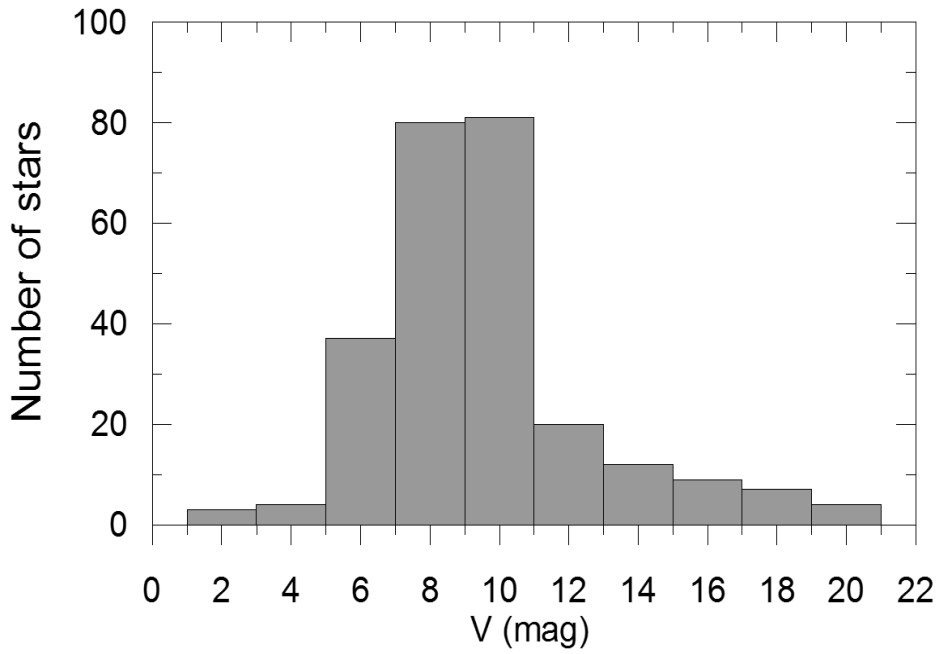


Figure 1: Apparent brightness distribution of 257 systems.

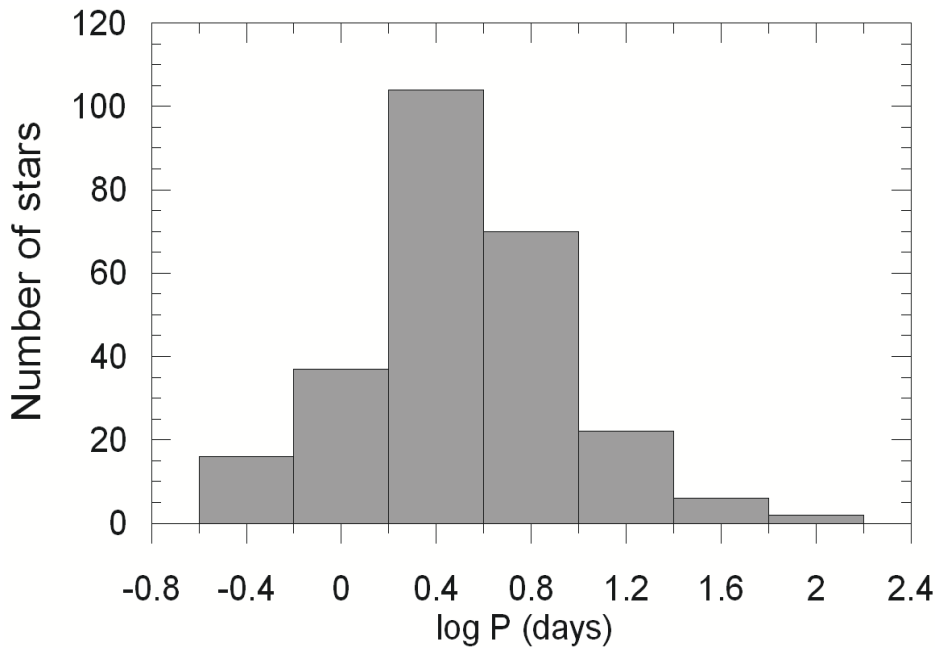


Figure 2: Orbital period distribution of 257 systems.

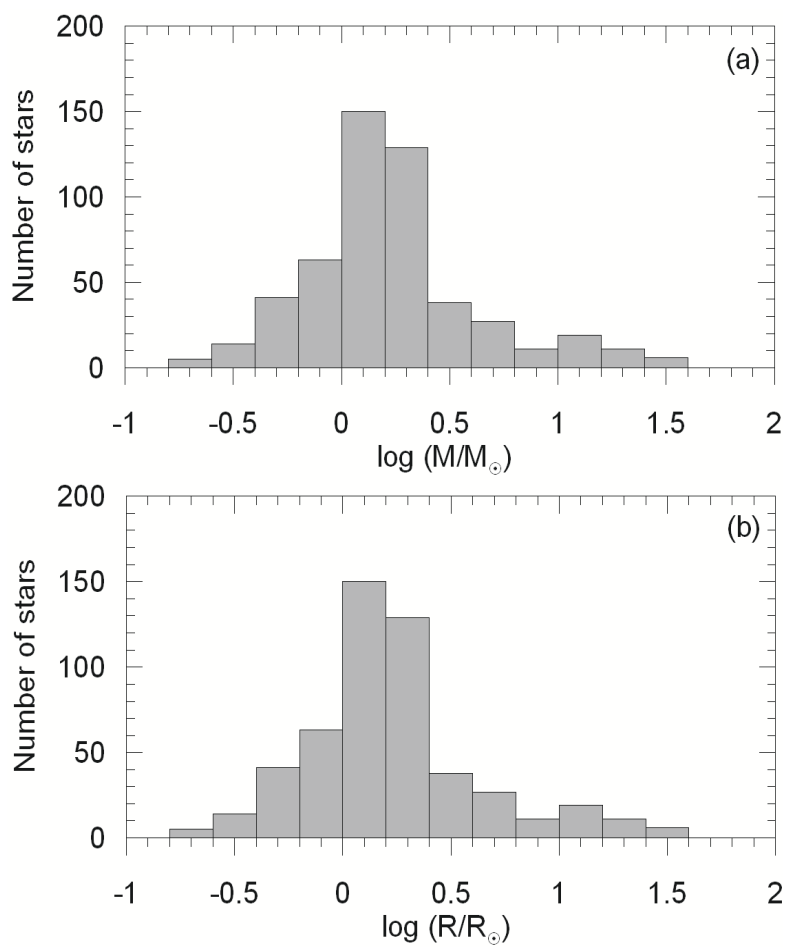


Figure 3: Distributions of masses (a) and radii (b) of 514 stars from 257 binaries.

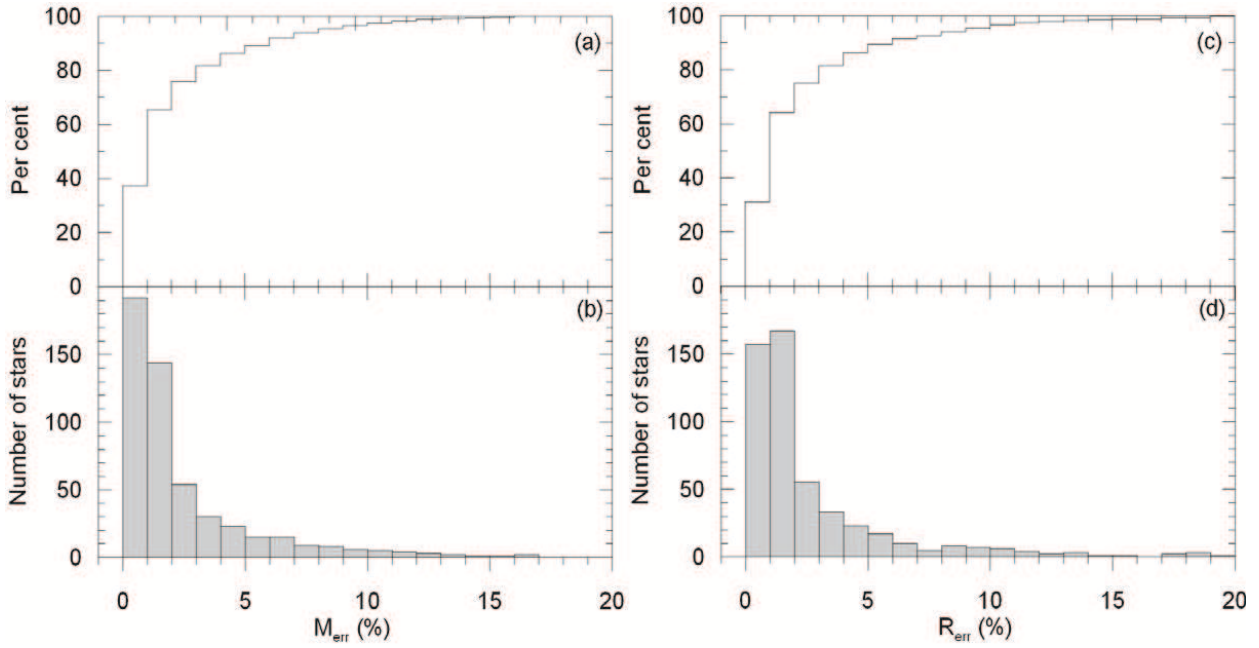


Figure 4: Uncertainty distributions of masses (a, b) and radii (c, d).

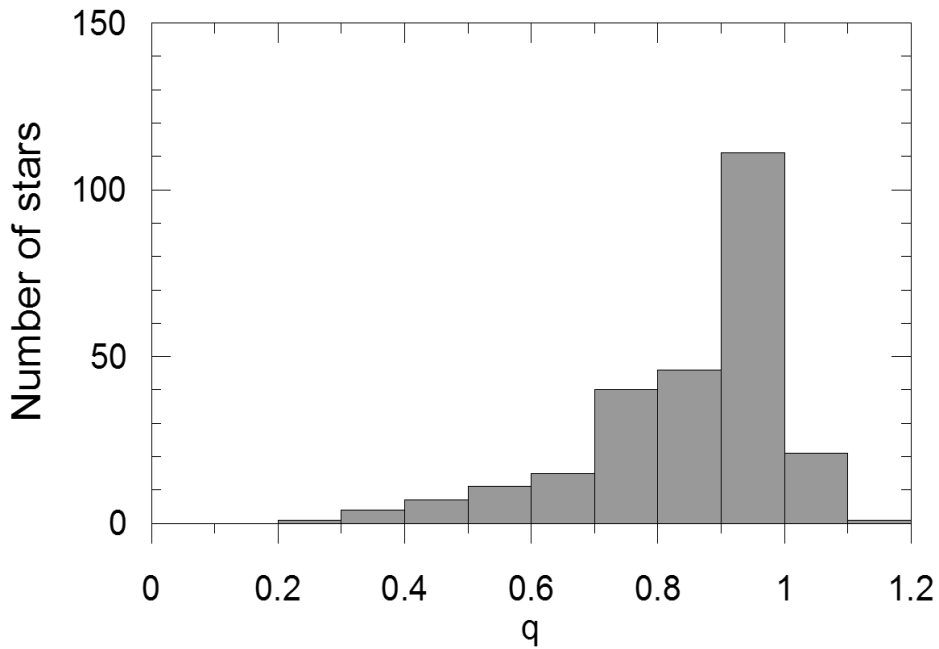


Figure 5: Mass ratio distribution of the sample. The median of q is 0.905.

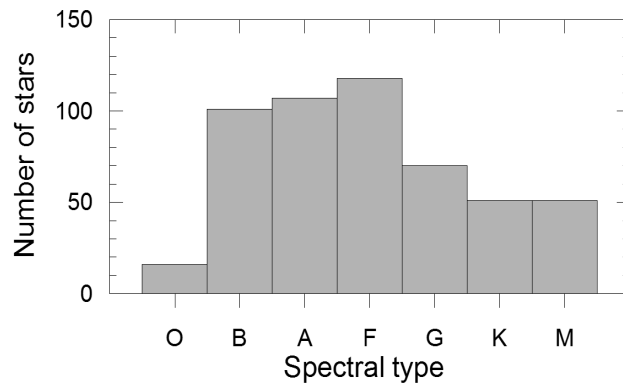


Figure 6: Distribution of 514 stars (257 pairs) according to spectral types.

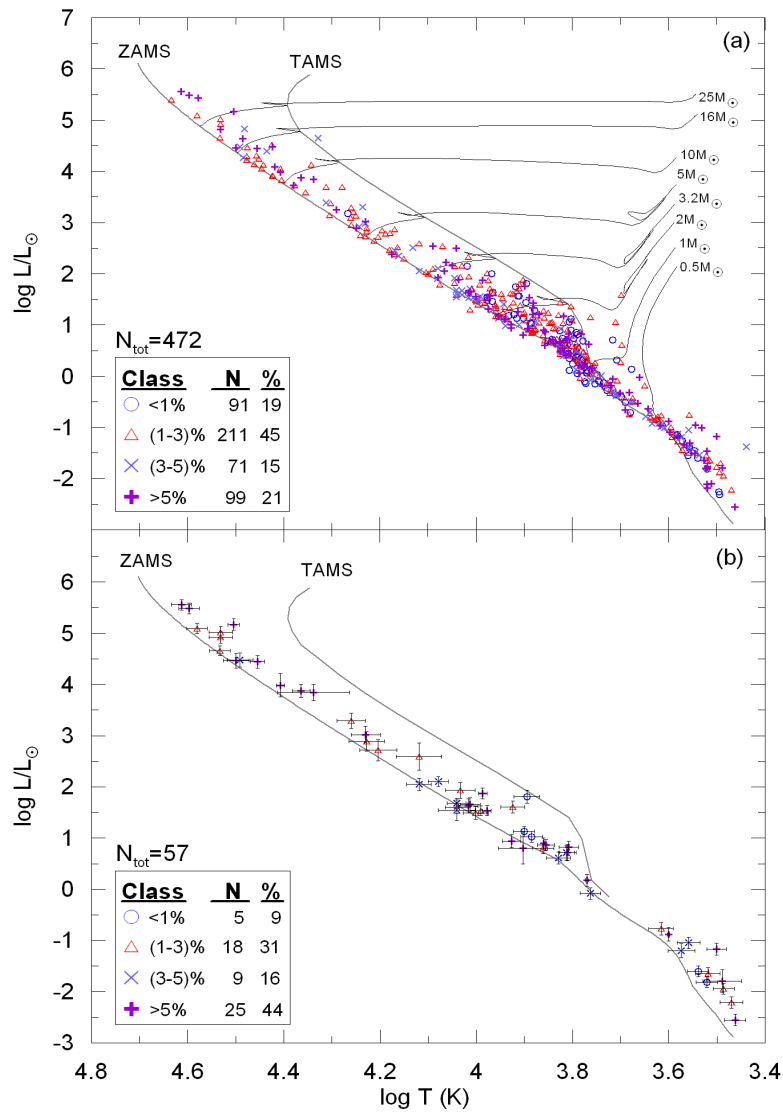


Figure 7: H-R diagram of 472 stars (a) and error bars (b) of 57 least accurate stars of the sample. Displayed error bars imply that most of the error bars in (a) are smaller than the symbols printed.

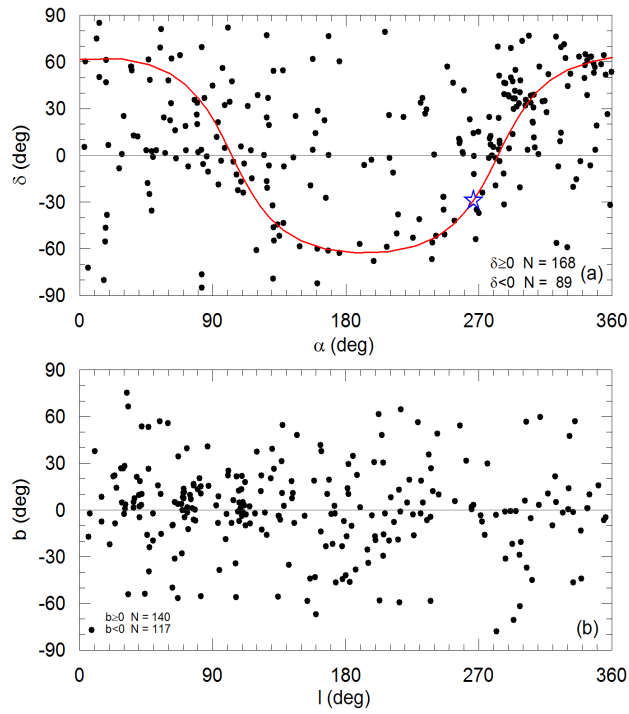


Figure 8: Distributions on the equatorial (a) and the Galactic (b) coordinates. Sinusoidal line in the upper panel is the Galactic plane, where the Galactic center is marked as a big star symbol.

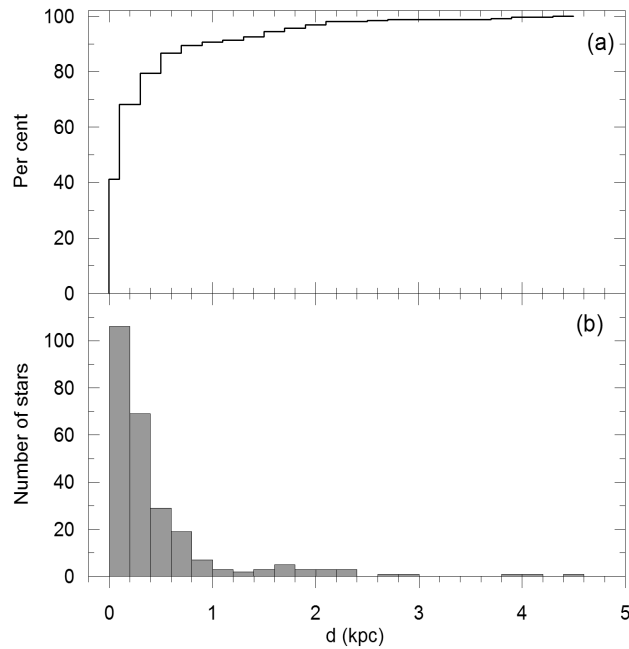


Figure 9: Distance distributions of the sample stars in the Solar neighborhood. (a) is in cumulative and (b) is in frequencies.

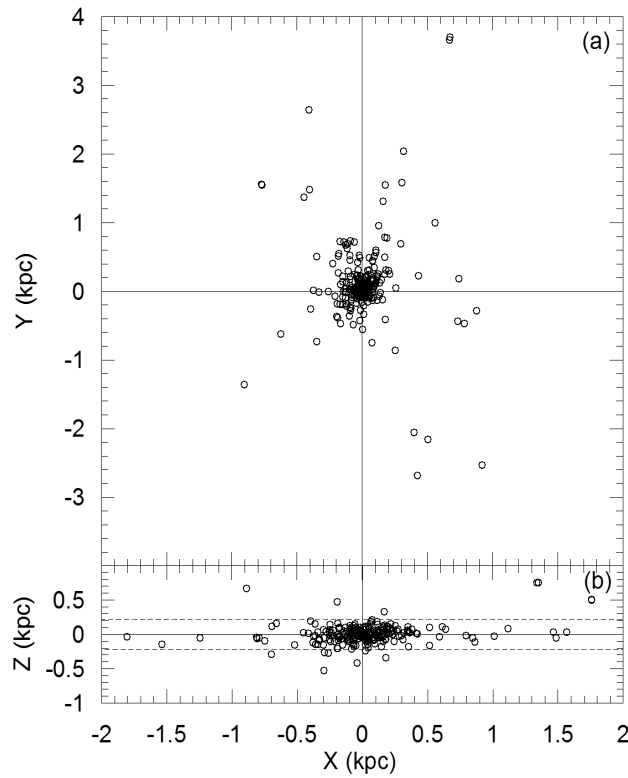


Figure 10: Distribution on the Galactic plane (a). X in the direction towards the Galactic center, Y in the Galactic rotation. Distribution on the plane (X - Z) perpendicular to the Galactic disc (b). Dashed line represents the scaleheight of the thin disc. The scaleheight of the thin disc ($H = 220$ pc) is taken from Bilir et al. (2006a,b).

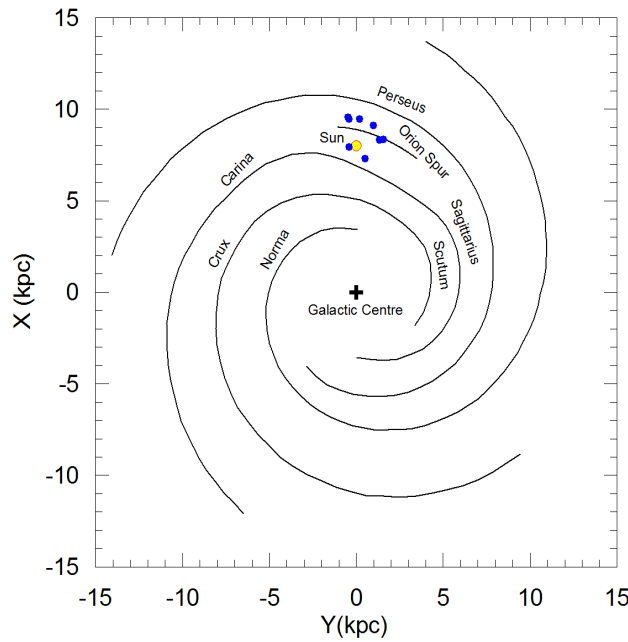


Figure 11: O-type binaries on the Galactic plane. The position of the spiral arms taken from Xu et al. (2009). It is assumed that the distance to the Galactic centre of the Sun is 8 kpc.

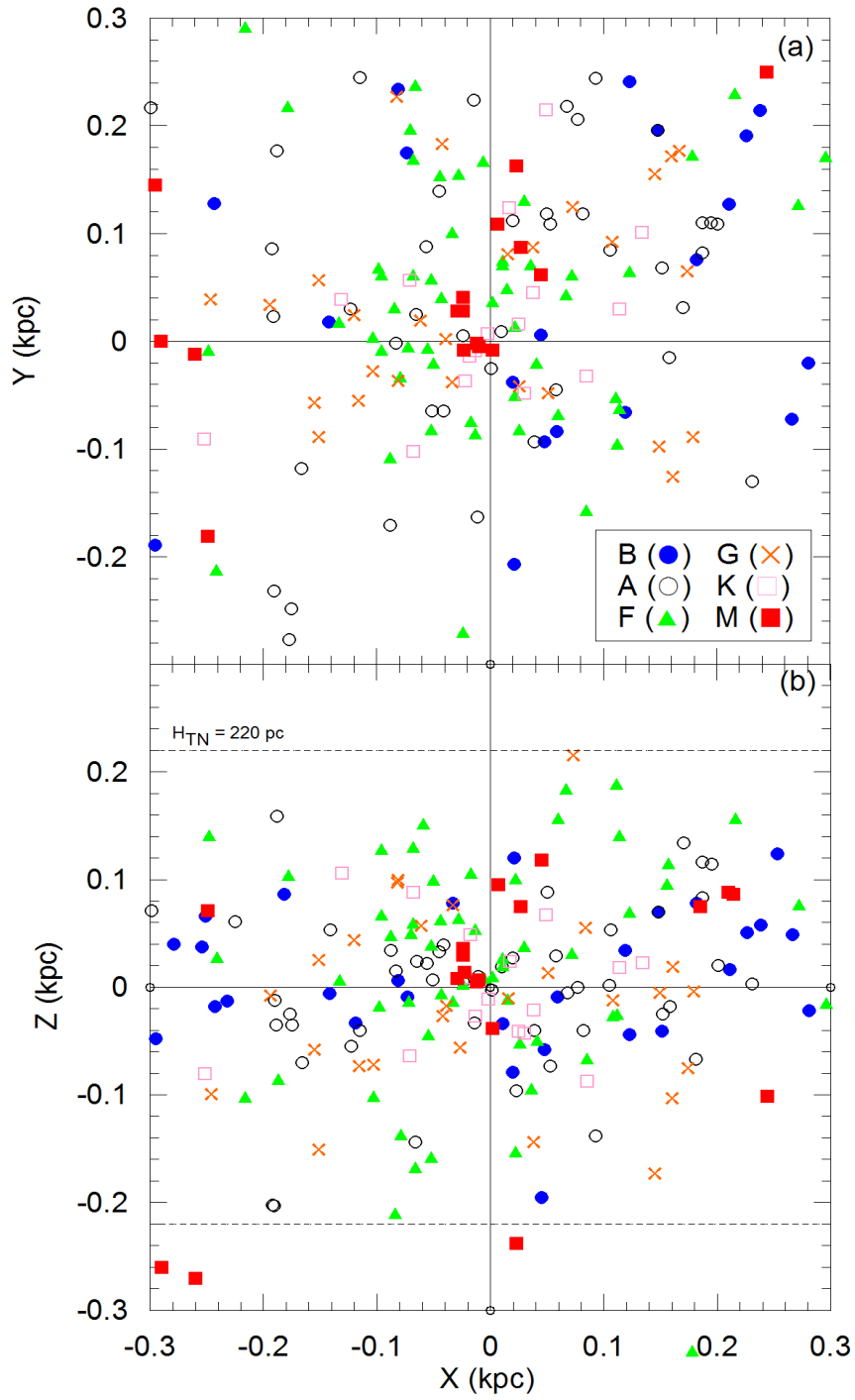


Figure 12: Nearby distributions of sample binaries within 300 pc.

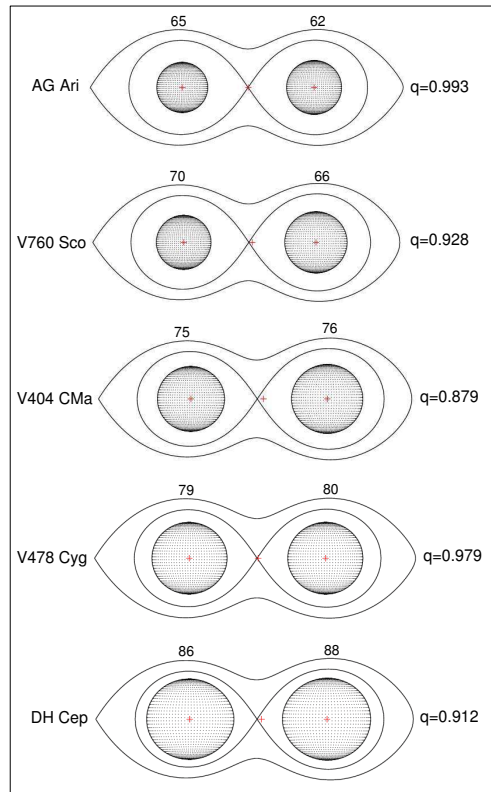


Figure 13: Examples of Roche lobe filling ratios. Names and the mass ratios are at the sides, while filling ratio (FF, Filling Factor) written on the top. By an eye inspection, one can notice sphericity spoils after filling factor 75.

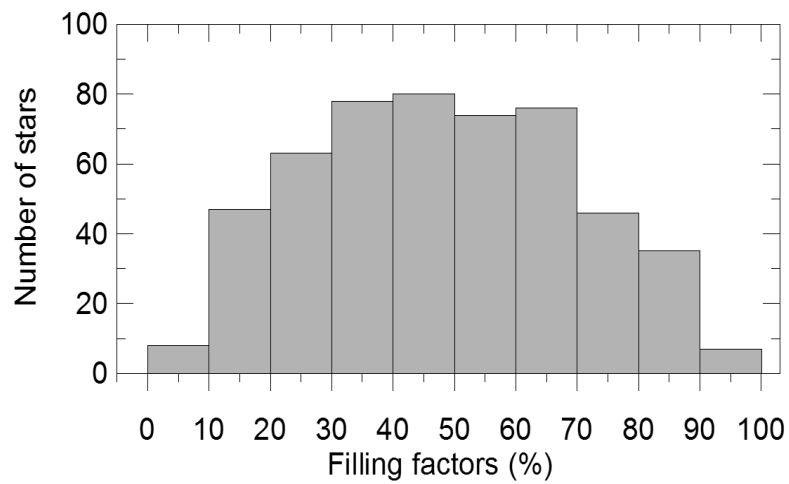


Figure 14: Distribution of the filling factors among 514 stars (257 binaries) of the sample.